Application of converted-wave 3D/3-C data for fracture detection in a deep tight-gas reservoir

TANG JIANMING, HUANG YUE, and XU XIANGRONG, SINOPEC
JOHN TINNIN and JAMES HALLIN, ION Geophysical/GX Technology

The deep-gas reservoirs of China's western Sichuan Basin are in Members 2 and 4 of the Upper Triassic Xujiahe Formation. These reservoirs contain mid- to large-sized gas fields like Xinchang, Hexingchang, Qiongxi, Zhongba, and Bajiaochang. The favorable geological conditions for creating these fields include abundant source rock, well-developed reservoir rock, good preservation conditions, and structural traps.

These reservoirs also have very low porosity and permeability, high pressure, complex gas-water relationships, and complex reservoir heterogeneity, which make it challenging to use conventional seismic technologies to predict and identify the complex reservoir and fracture systems. However, multicomponent seismic technology can acquire converted-wave data that reflect rock matrix information and anisotropy and P-wave data that reflect matrix and fluid characteristics. This article describes how this technology solved such problems as identification of high-quality reservoirs and detection of fractures and its potential for determining fluid characteristics in the deep-gas reservoirs of the western Sichuan Basin.

Geologic setting

Sichuan Basin covers about 180,000 km^2 within the upper Yangtze deposition zone. The periphery of the basin is deformed by thrust zones and contains marine and continental sedimentary facies with a thickness of 6000–12,000 m. This thick sequence consists of organic-rich source rocks from upper Sinian to Jurassic with favorable conditions for oil and gas generation, migration, storage, and preservation. Gas reservoirs occur in the Sinian, Ordovician, Carboniferous, Permian, Triassic, Jurassic, and Cretaceous sedimentary deposits. Estimated total volume of gas resources in the entire Sichuan Basin is 212 TCF, and this middle section in western Sichuan contains 43 TCF (Zhengwu, 2004).

Basic characteristics of Xujiahe Member 2 reservoirs

Figure 1 shows the reservoirs in Xujiahe Member 2, which formed as sand bars at the front edge of the delta and as channels within the delta plain. Reservoir depth is typically around 5000 m.

Core analysis, well logging, and microscopic identification on thin sections show three types of reservoirs: porous, fractured-porous, and fractured.

The fractured and fractured-porous reservoirs have matrix porosity generally below 4%, and most samples show porosity below 3% with matrix permeability less than 0.1 millidarcy. The porous reservoirs generally have porosity higher than 4%.

Drilling revealed that the most common reservoirs are fractured-porous followed by fractured reservoirs and then porous. Production varies greatly depending on the type of reservoir. Well CG561, in a porous gas reservoir, produces around 0.96 MMCF/d; wells X851, X856, and X2, in fractured porous reservoirs, produce around 17.66 MMCF/d.

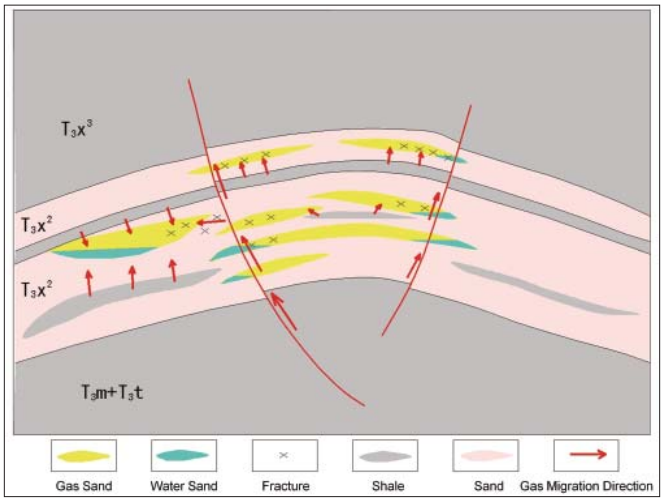

Figure 1. *Reservoirs of Member 2 of the Upper Triassic Xujiahe Formation in Xinchang gas field.*

Reservoir log-response characteristics

Log analysis of well CX560 reveals a gas reservoir at 5161.6–5171.8 m. FMI images show developed reservoir fractures; however, the matrix porosity is very low, which indicates that the reservoir is rather tight.

Well CX565 penetrates a porous reservoir, and log analysis shows good gas-bearing response at 4942–4960.6 m. FMI data reveal no obvious fractures, indicating that the reservoir is porous.

Examples of the prolific fractured-porous reservoirs are wells X851, X856, and X2. All have the high production rates mentioned above.

Both conventional and full-wave sonic logs reflect the fractured reservoir characteristics of well X851 at depths of 4831–4836 m and 4842–4846 m.

The ARI and FMI images of well X856 clearly reflect effective fractures at 4820–4825 m. FMI images show both effective and ineffective fractures in the borehole wall, whereas ARI images show only fractures with radial extensions greater than 2 m. Comparing the FMI and ARI images enables estimation of radial extensions of factures and identifying their effectiveness. Analysis of FMI and ARI images shows well-developed vertical and net-like fractures in reservoir sections of this well.

Physical characteristics of reservoir rock

Physical rock characteristics, obtained from simulating high-temperature and high-pressure conditions, show obvi-

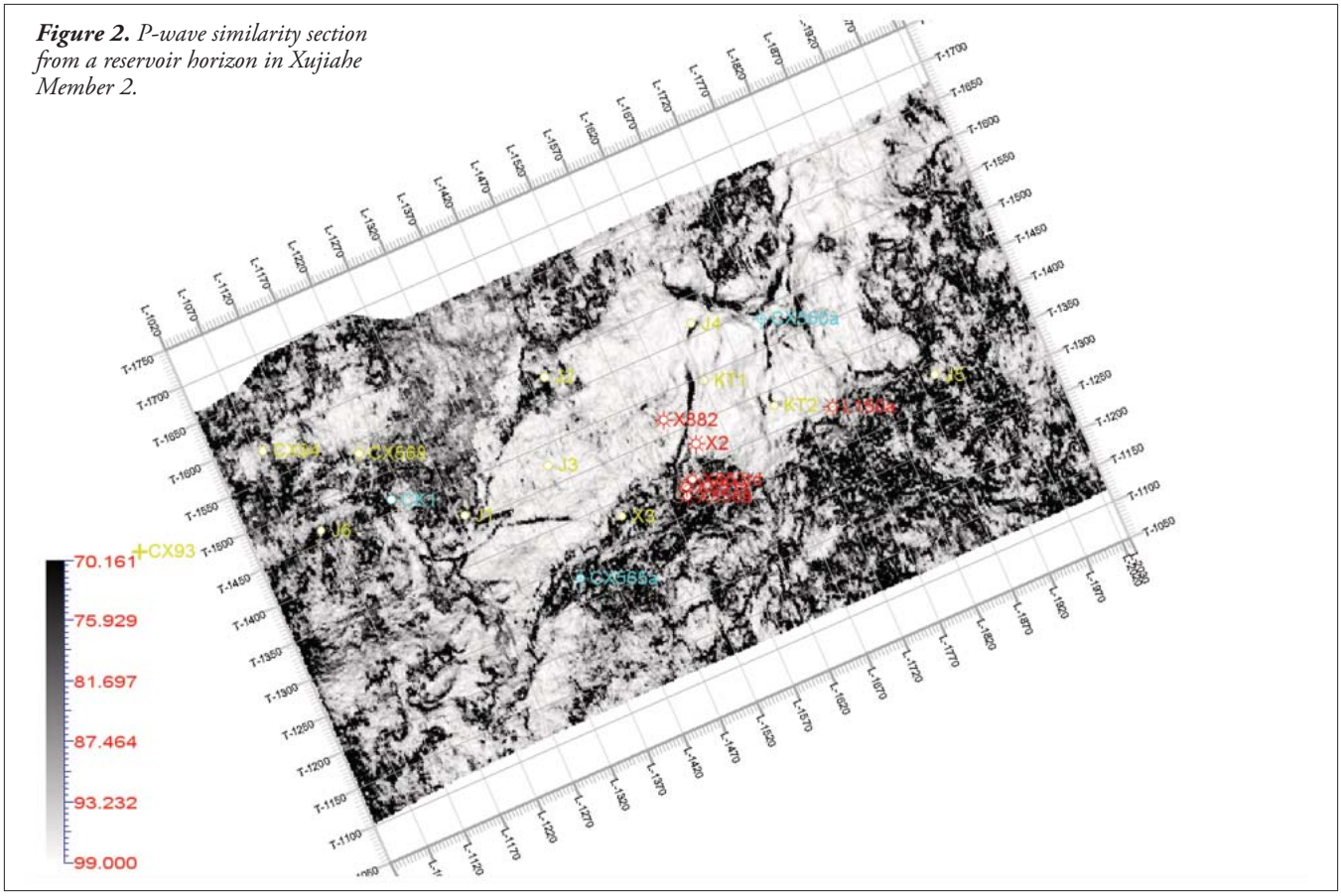

Figure 2. *P-wave similarity section from a reservoir horizon in Xujiahe Member 2.*

ous changes between water versus gas-saturated conditions. When sandstone reservoirs in Xujiahe Member 2 contain gas, the Lamé constant (λ) reflecting rock compressibility decreases, the shear modulus (μ) reflecting rock matrix remains unchanged, the ratio of P-wave to S-wave velocities decreases, and Poisson's ratio decreases below 0.27. Statistical analysis of rock types obtained from log analysis produces "distribution rules" for lithologies based on V_P/V_S, P-wave velocity, P-wave impedance, and density. P-wave velocity and impedance are generally low in gas-bearing sandstones and high in water-bearing and tight sandstones. However, it is difficult to distinguish gas-bearing sandstones from other rock types using P-wave impedance only. The density of gas-bearing sandstones is on the low side but overlaps the water-bearing and tight sandstones. Full-wave attributes, like the distribution of V_P/V_S, make it easier to distinguish gas-bearing, water-bearing, tight sandstones, and shales. Gas-bearing sandstones have an overall V_P/V_S ratio on the low side, 1.55–1.65; shales are 1.7–1.8. Therefore, using P-wave and S-wave information improves the prediction of gas-bearing reservoirs.

Fractures, especially high-angle, dual-direction intersecting fractures, are necessary for the highest production in western Sichuan, and this geologic complexity makes it challenging to explore for deep-gas reservoirs using conventional seismic technology. However, 3D/3-C technology—including P-wave and C-wave processing, inversion, full-wave attributes analysis, and comprehensive interpretation of multicomponent data—enable the identification of high-quality reservoirs and detection of fractures.

3D/3-C converted-wave exploration

Acquisition. The recording geometry and acquisition parameters used for converted-wave 3D/3-C exploration in Xinchang were: recording geometry of 12 L × 16 S × 264 R; bin size of 25 × 25 m; fold 66; 3168 receivers per shot; receiver and source spacing of 50 m; receiver line spacing of 400 m; source-line spacing of 300 m × 2; aspect ratio of 0.7; inline array = 6575 – 25 – 50 – 25 – 6575.

This recording geometry provided good azimuthal coverage for all offsets to a maximum of 6000 m.

Processing. The 3D converted-wave processing included:

1) Processing each component (vertical, radial, and transverse) separately but using P-wave data to constrain parameters in areas where it is most reliable. Examples of using P-wave and S-wave data jointly include C-wave statics corrections and attenuation of surface-wave noise.
2) Processing data from the different components, both isotropically and anisotropically, to provide input for reservoir prediction, gas-bearing analysis, and fracture detection.
3) Simultaneous prestack P-wave inversion and joint or dual prestack inversion of P-wave and S-wave data using the anisotropic processed data.
4) Application of the azimuth-sectoring approach to enable

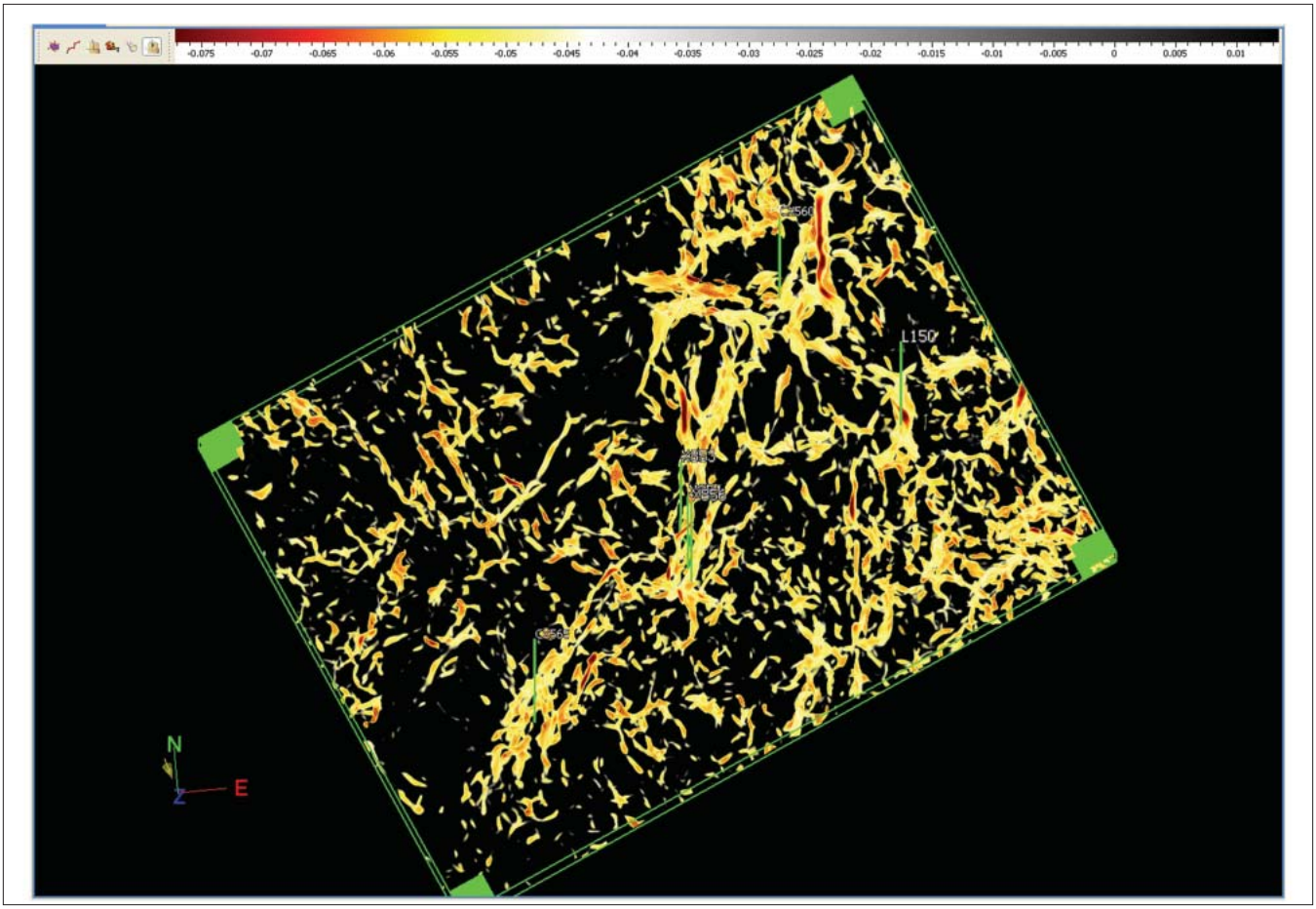

Figure 3. *Results from P-wave curvature.*

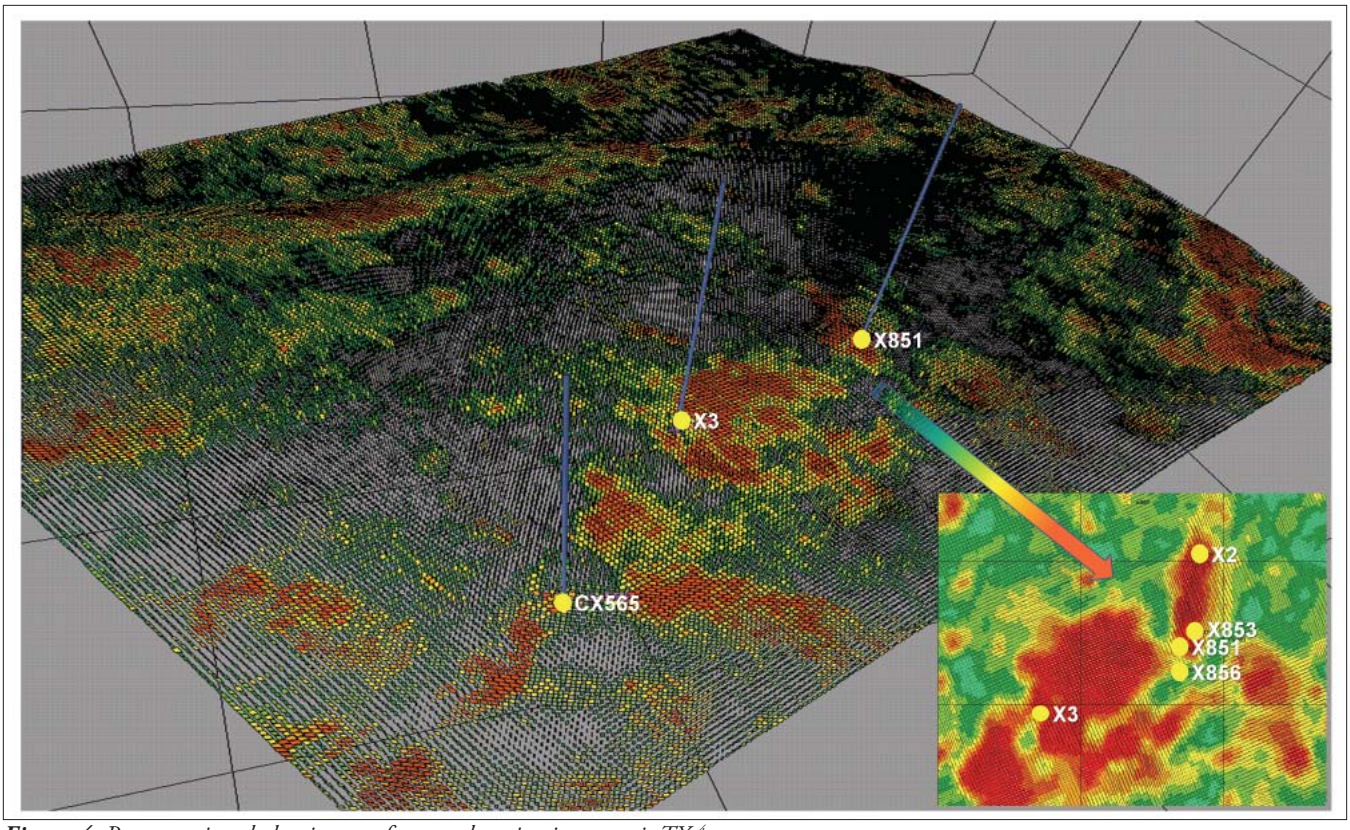

Figure 4. *P-wave azimuthal anisotropy fracture detection in reservoir* TX_2[4].

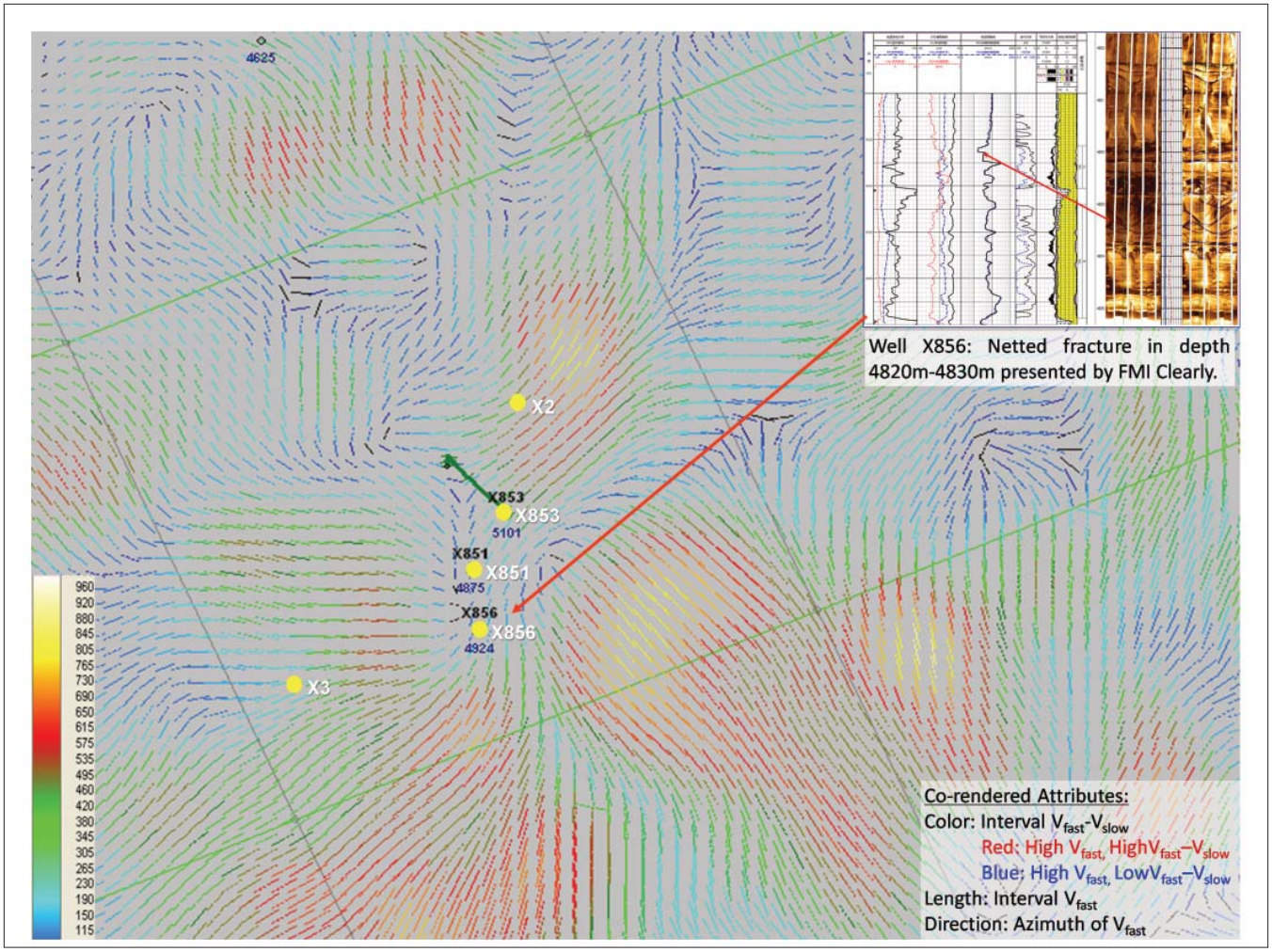

Figure 5. *Diagram of P-wave VVAZ fracture detection in reservoir TX_2^4.*

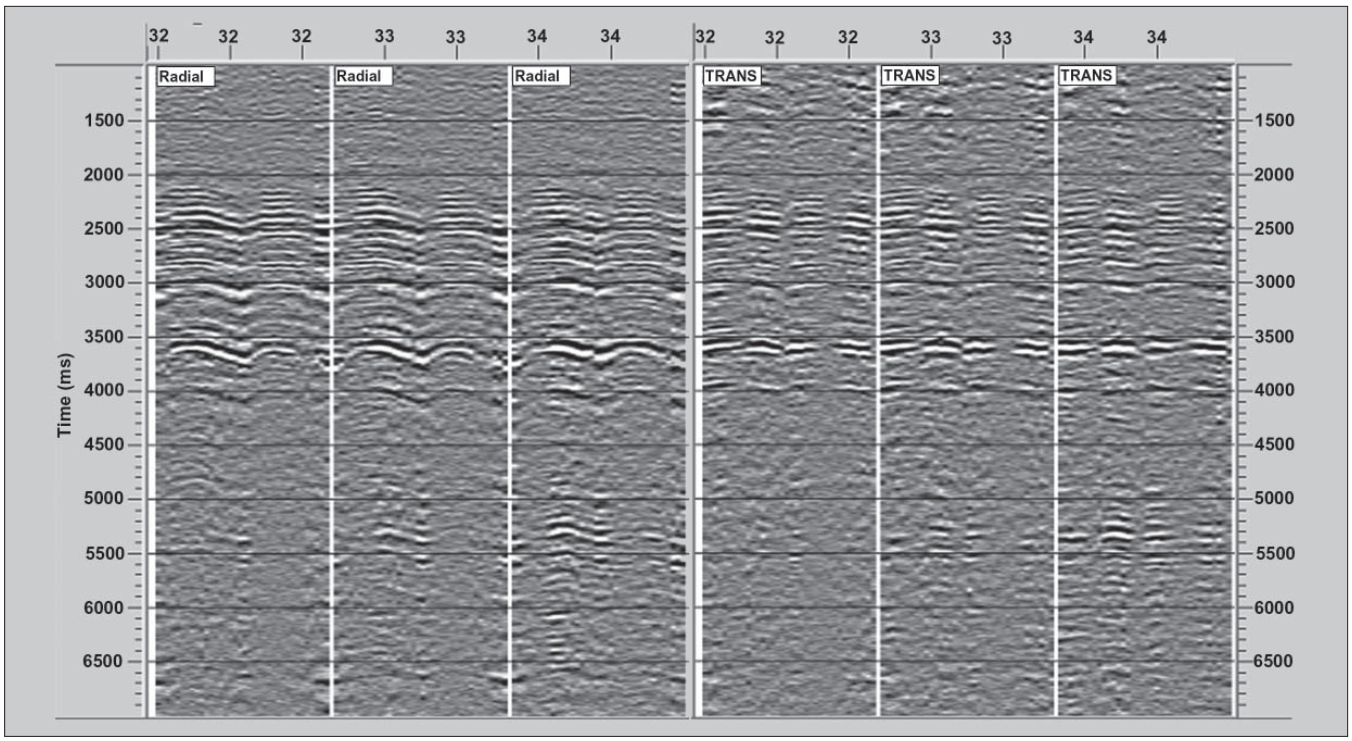

Figure 6. *Azimuthal sectored gathers of the radial component and transverse components.*

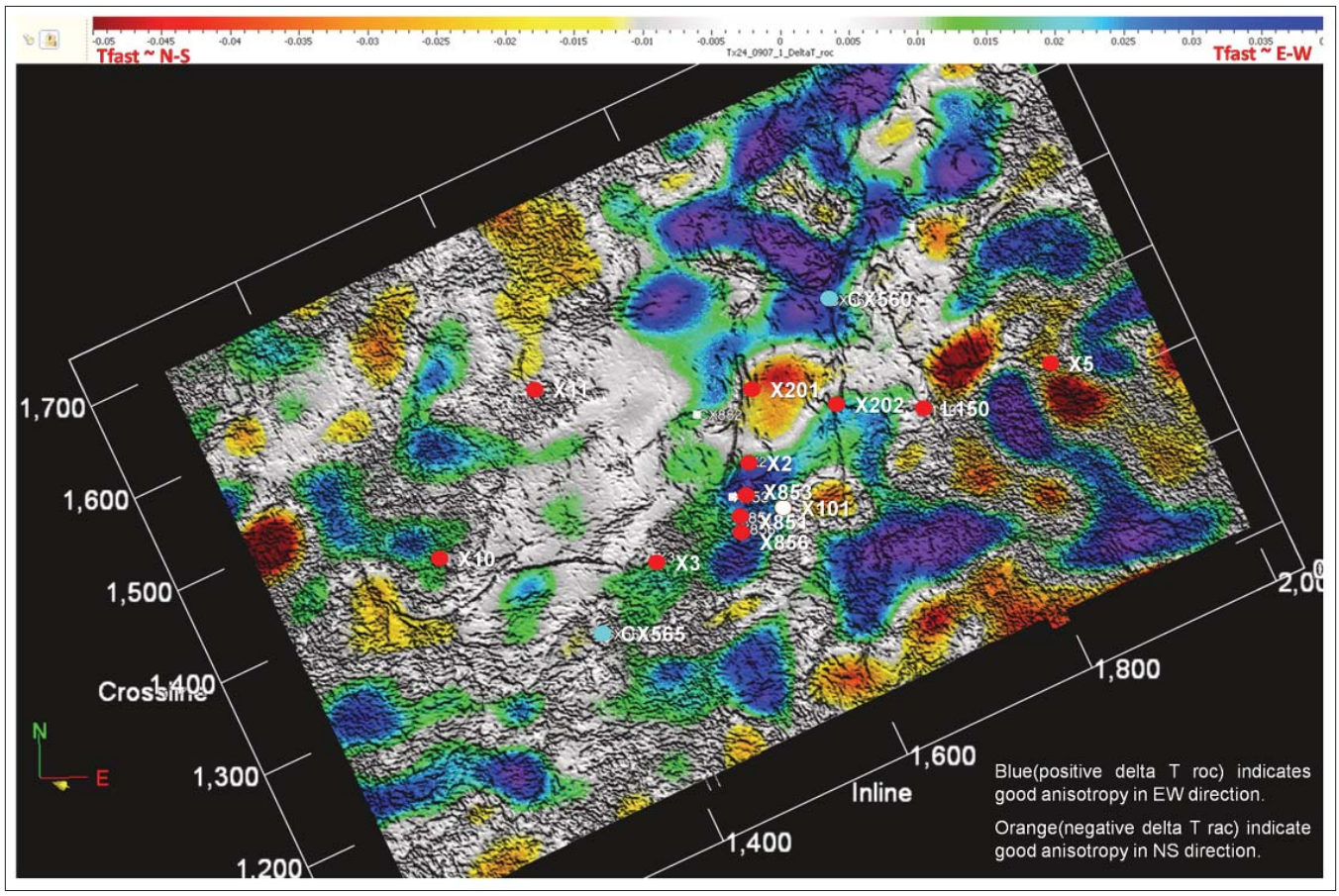

Figure 7. *Time delay rate of change along reservoir TX_2^4.*

equally partitioned prestack time migration of azimuth gathers for the vertical, radial, and transverse components. The azimuthal data are essential for fracture detection using P-wave anisotropy and C-wave splitting analysis.

5) Rotation analysis and layer stripping on azimuth-sectored radial and transverse data to provide fast and slow shear-wave volumes for fracture orientation and density calculation, as well as reservoir prediction studies.

Interpretation. The key steps include: calibration of P-wave and S-wave data with well information; registration of P-wave and S-wave data; joint inversion of P-wave and S-wave data; analysis of full-wave attributes; and detection of fractures.

Joint P-wave and S-wave interpretation provides more precise information than interpreting them separately. The advantages of converted-wave interpretation include:

- More accurate structural imaging. In the case of "gas clouds," converted waves can image structures that P-waves cannot.
- Good lithologic discrimination. Sandstones and shales can be distinguished using V_P/V_S or the Lamé constants and shear modulus.
- More reliable prediction of quality reservoirs. The use of elastic impedance, V_P/V_S, Poisson's ratio, and density helped predict reservoir quality.
- Fluid identification capability. Based on rock properties and well logs, parameters such as V_P/V_S, the Lamé constants, shear modulus, and Poisson's ratio can identify fluid content.
- Multiple fracture detection methods. Wide-azimuth multicomponent data enable the use of many fracture-prediction techniques, including methods based on regional tectonic and structural analysis, seismic attributes, P-wave azimuthal anisotropy, shear-wave splitting, and fracture modeling. Integrating these techniques significantly improved fracture prediction.

Full-wave fracture detection

Figure 2, a P-wave diagram of a similarity section from Xujiahe Member 2, clearly shows the distribution of main fractures, small faults, and fracture swarms near faults, which are difficult to find using conventional structural interpretation. Production information shows that wells in the chaotic zones of the similarity slices have the highest production rates. Image logs from these wells confirm higher fracture density in the reservoir zones.

Calculating 3D curvature attributes is done by choosing a subvolume centered on a point in the P-wave data volume, automatically picking peak values or zero crossing points at the central point, correlating with adjoining traces using least squares or fitting with other methods, and solving the second derivative to obtain the curvature of the central point. Figure 3 is a 3D opacity diagram of P-wave curvature of Xinchang

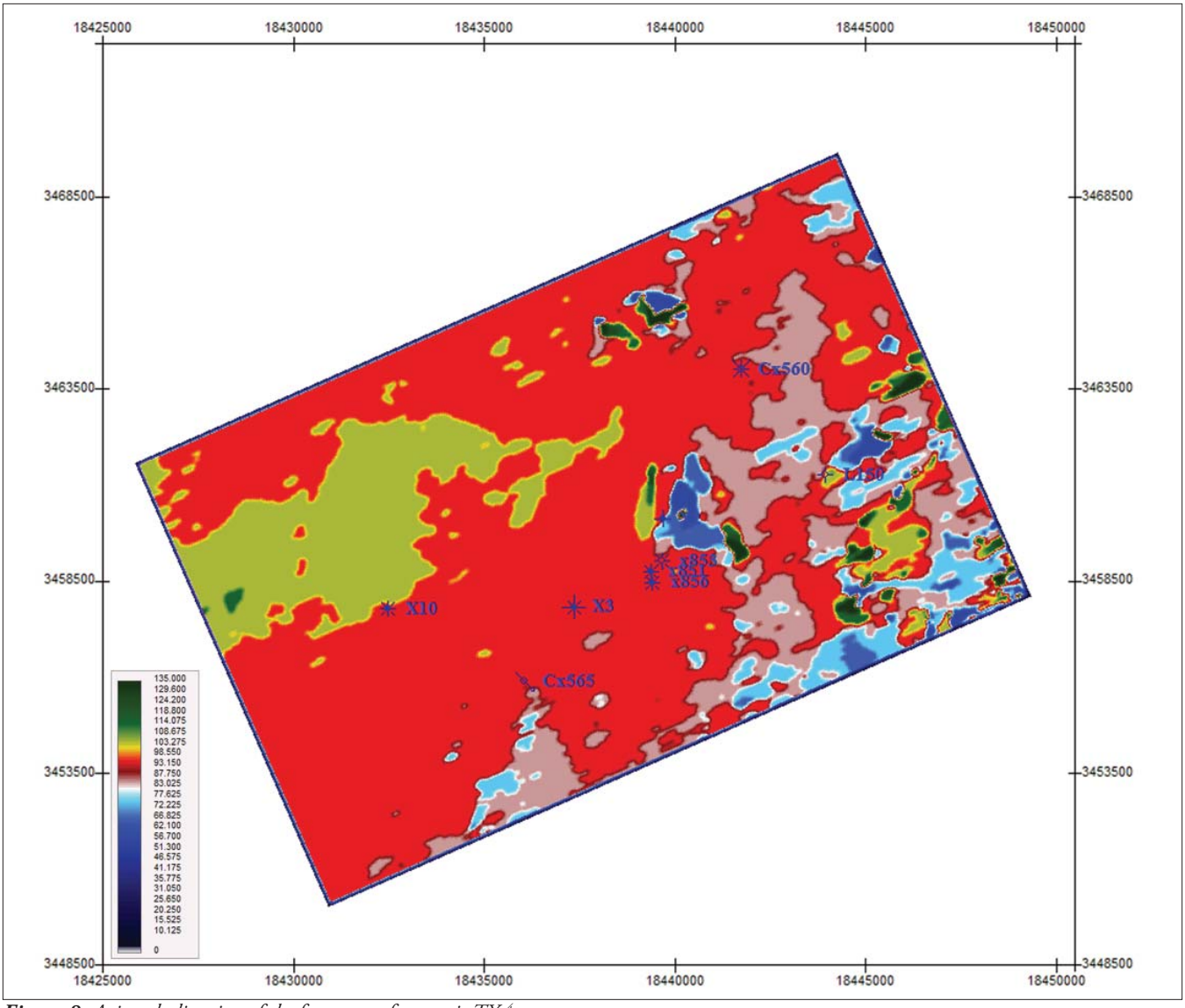

Figure 8. *Azimuth direction of the fast wave of reservoir TX_2^4.*

with high curvature values indicating the fracture network.

Fracture detection by P-wave azimuthal anisotropy

This technology uses changes in amplitude, velocity, propagation time, and AVO attributes to predict orientation and density of fractures (especially vertical or high-angle fractures). The prediction results are often linked to microscopic fractures.

AVAZ fracture detection is based on changes in P-wave amplitude with azimuth (Jenner, 2001). Wells X2, X853, and X3 in Figure 4 are in the zone with the highest predicted fracture density, which is related to single-direction fracture zones. Wells X851 and X856 have dual-direction fractures and high production rates, even though the figure shows them in a zone of low fracture density, because AVAZ is inefficient at imaging fracture network systems. Theoretically, it is difficult to reflect the true fracture development in the case of dual-direction fractures using AVAZ or AVOAZ because the difference is anomalously small in all directions.

Azimuthal anisotropy of P-wave propagation velocity has a lower vertical resolution than AVAZ; however, it is important for P-wave azimuthal fracture prediction because of its reliable reflection of overall macroanisotropic features. Figure 5 shows the 3D/3-C P-wave VVAZ analysis results of TX_2^4. Both Vfast and Vfast-Vslow are low near wells X851 and X856, indicating dual-direction fractures. However, around well X853, the red parts have high Vfast and Vfast-Vslow, indicating single-direction parallel fractures. The blue zones with longer line segments are without fractures.

S-wave splitting fracture detection

S-waves split when passing through anisotropic media (fractures). Propagation is fast when particles vibrate parallel to fractures and slow when vibrating perpendicular to fractures. The strike of fractures can be located precisely by identifying the direction of fast S-wave. The time difference between the fast and slow waves is indicative of fracture density.

Significant evidence indicating fracture development is

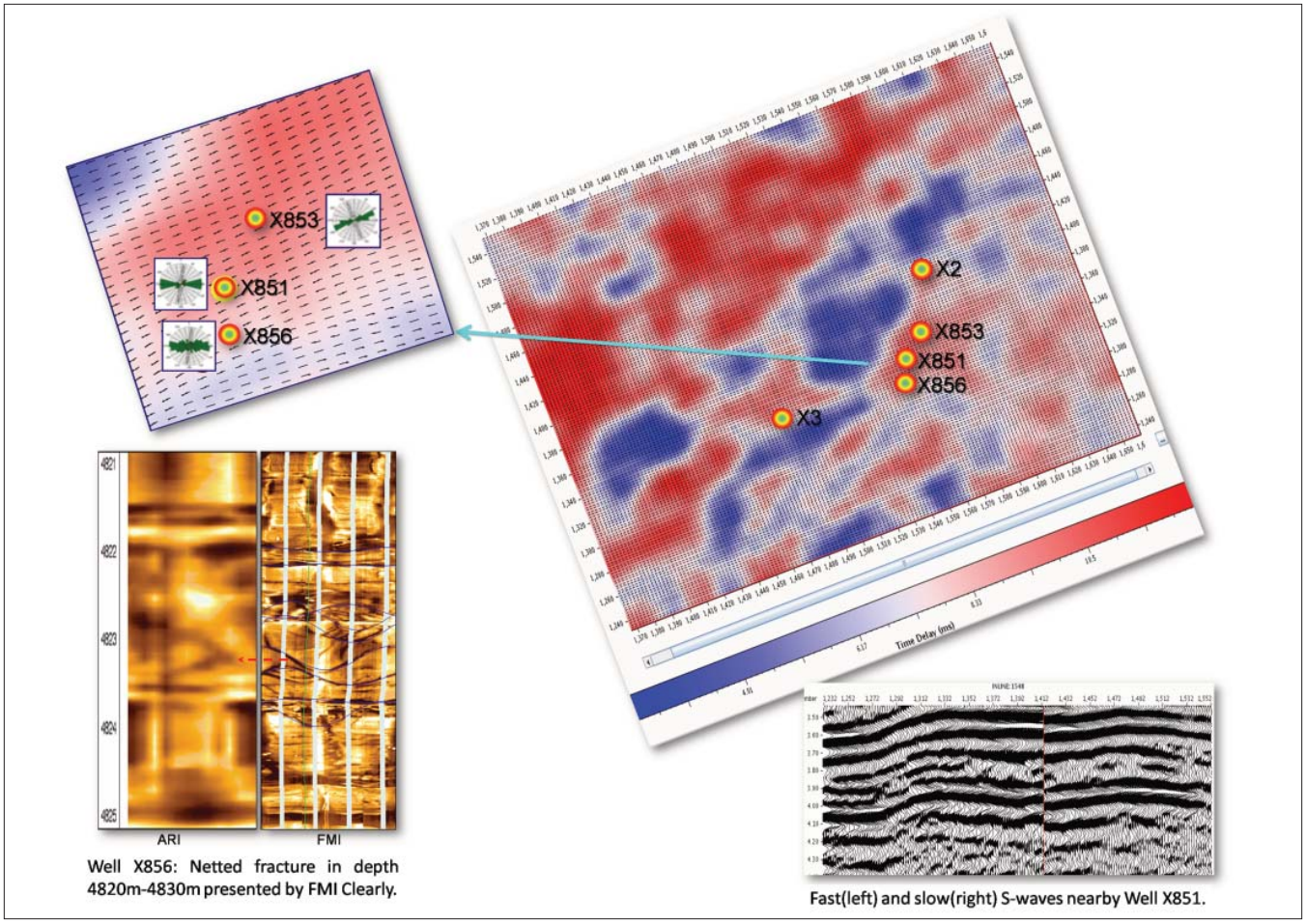

Figure 9. *Fracture development azimuth and density in reservoir TX_2^4 through S-wave splitting detection.*

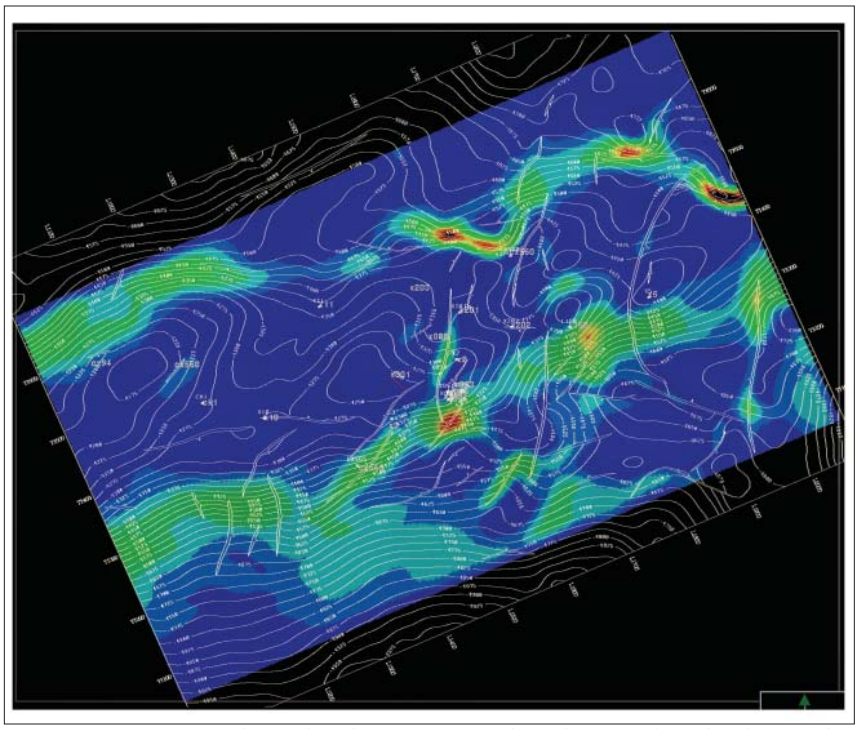

Figure 10. *Fracture prediction based on cumulative-dependent variables of geohistory of reservoir TX_2^4.*

present in C-wave records of Xinchang. Figure 6 shows azimuthal sectored gathers of radial component and transverse component. Each trace of the six gathers shown represents a migration of a 10° azimuth sector; thus, there are 36 traces or azimuths for each gather. The three left panels display a gather after azimuthal sectoring of the radial component data, showing the radial component records have noticeable changes of time and amplitude with azimuth. The sinusoidal appearance is typical of anisotropic media such as fractures, and the time difference within the sinusoid is the ΔT. The three right panels exhibit the azimuthal gather after sectoring of the transverse component, which shows that the transverse data has strong energy in the target reservoirs, indicating severe anisotropy of the formation. The evident reversal of polarity every 90° indicates the fast and slow directions within 10°, thus providing accurate fracture orientation.

Relative time difference method. The steps for calculating S-wave splitting time delays are:

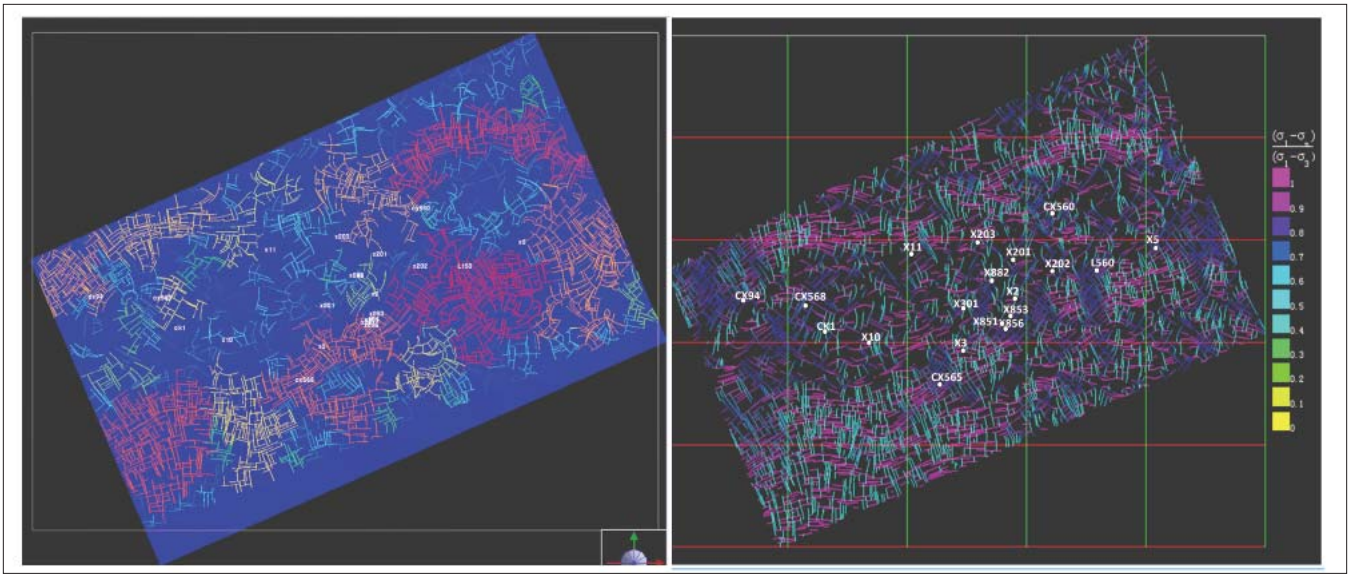

Figure 11. *Prediction of interconnecting units and expanding tendency of fractures in reservoir TX_2^4.*

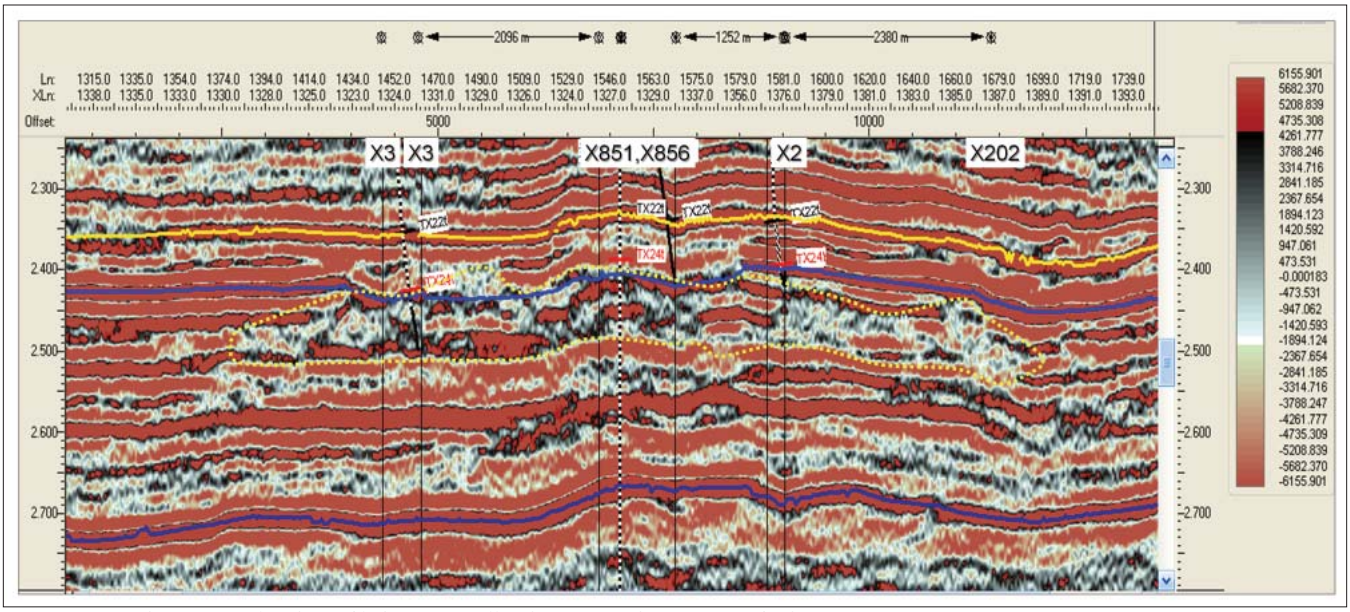

Figure 12. *Arbitrary amplitude profile between wells (characterized targets in off-white).*

1) Obtain the direction of regional anisotropy (fast direction) through angle scanning and time differences.
2) Rotate the radial and transverse components to the azimuths of the fast and slow directions.
3) Cross-correlate fast and slow waves to calculate angle and time delays.
4) Obtain the rate of change in delay time difference by computing the gradient of the time delay.

Figure 7, a relative time difference map of primary reservoir horizon TX_2^4, shows that high-producing wells are generally in zones with larger time delays. Figure 8, the fast shear-wave direction of reservoir horizon TX_2^4, shows that most azimuths are close to EW, which correlates with the principal stress direction derived from borehole breakout information in the area.

Layer-stripping method. S-wave splitting effects on the 3D/3-C data were evaluated and corrected using a layer-stripping method. Areas in which the corrections were necessary and the amount of the correction provided valuable information for the prediction of fracture zones. Figure 9 shows that the main direction of fractures of well X851 is EW (with azimuth at about 90°), and the time delays at well X851 are up 40–50 ms. The large time delays indicate considerable fracture development and coincide with drilling results.

Geotectonic history analysis on fracture effectiveness

One approach to fracture prediction is tracing basin stress history through reconstruction of sequential tectonic movements. Such parameters as fracture growth and density are then derived from a stochastic simulation controlled by multiple parameters (stratum thickness, lithology, fracture propagation direction, etc.). The ultimate objective is to predict zones of high-fracture density and fracture directions.

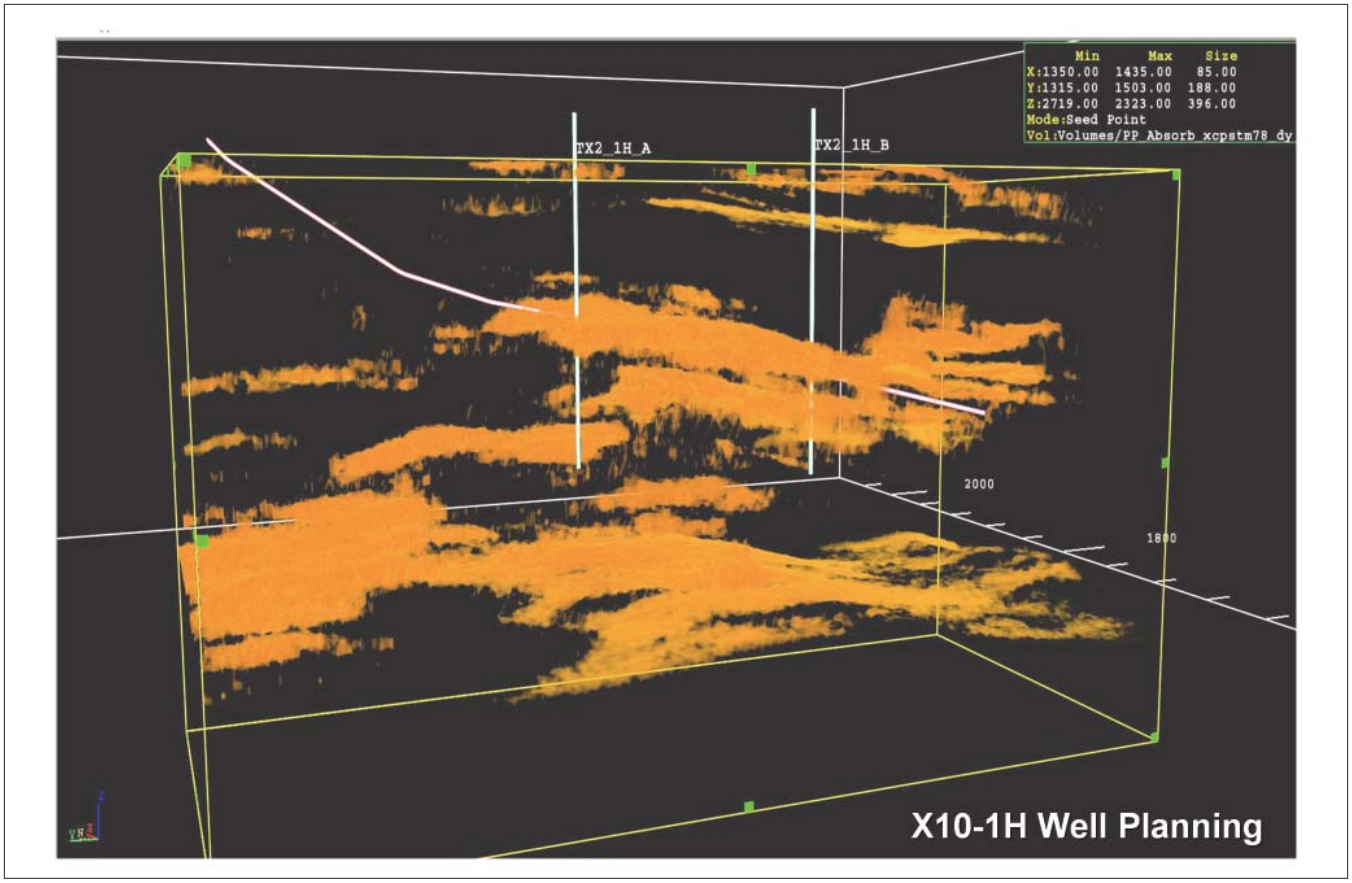

Figure 13. *Connected bodies of reservoir TX_2^4.*

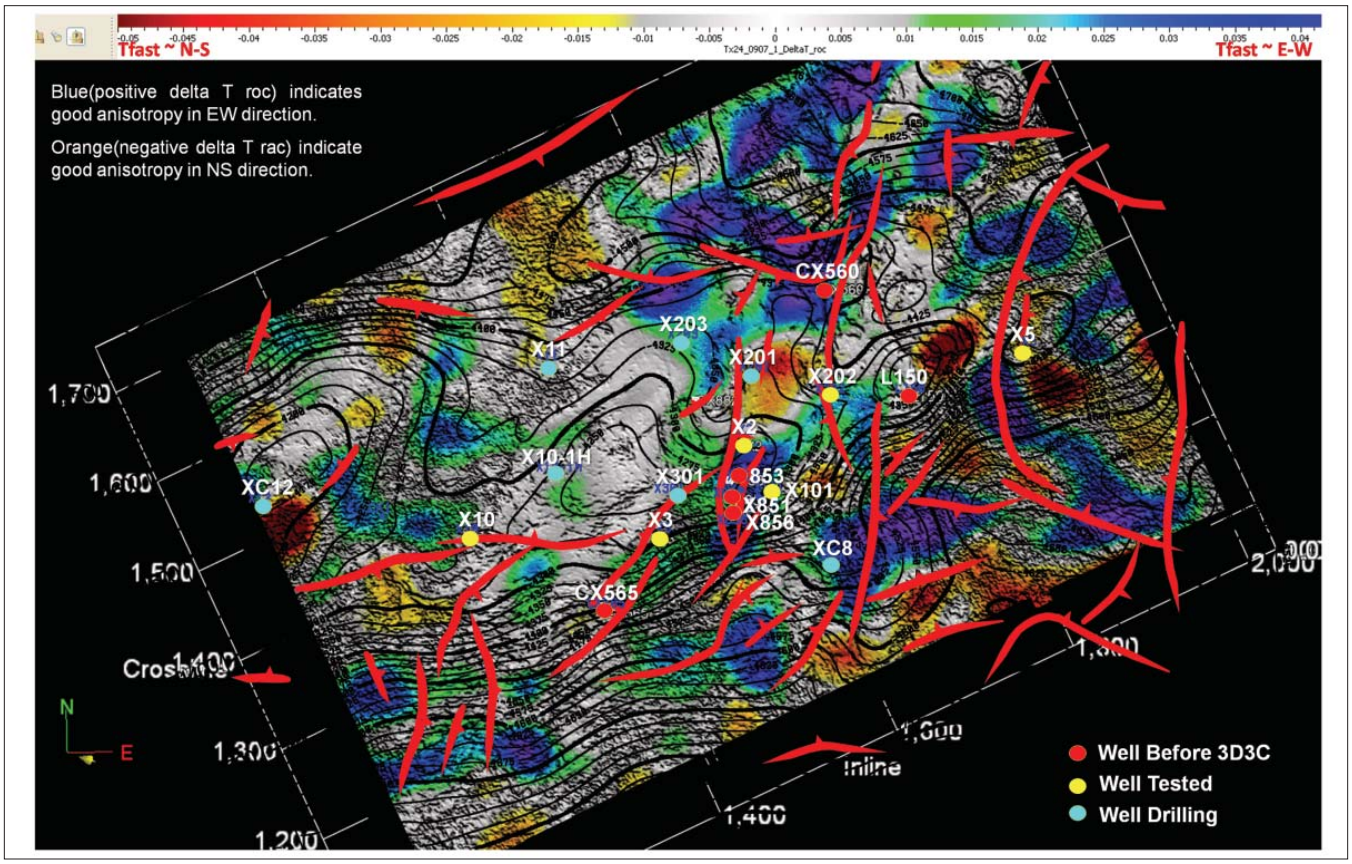

Figure 14. *Well locations resulting from integrated fracture data analysis.*

Wells drilled in the Xujiahe Formation include X851, X853, CX560, CX565, and L150. Wells X851 and CX565 have the most developed fractures found during drilling in recent years. Wells X853 and CX560 have relatively developed fractures; well L150 has poorly developed fractures.

In Figure 10, the areas with favorable fracture development are in the north and south flanks of the structure. The south flank includes wells X851 and CX565, the area south of these wells, and area south of well L150. The north flank includes well CX560. Structurally, well X851 is in the structural high, within a well-developed fracture zone. Well CX560 and the section to the north have gentle to steep dips where orthogonal fractures exist. These steep flank areas have developed fractures, whereas higher and flatter positions show less fracture development. Wells X10 and X11, in the structural high, have only moderate- to low-angle fractures and bedding fractures, which indicates that the stress-based prediction of the fractures is accurate.

Fracture prediction based on evaluating geohistorical stress through basin reconstruction should macroscopically show large-scale fracture development. Fractures in higher, flatter areas are not as easy to predict with these methods. Thus, fracture prediction using full-wave seismic attributes has an obvious advantage in predicting the degree of fracture density in the flatter areas. Additionally, the accuracy of the fracture orientation information from the shear-wave splitting analysis is crucial for the well to intersect the maximum number of fractures.

Figure 11 (left) shows calculated connectivity of fractures (units of the same color indicate the same fracture network system). The right side is a diagram of expansion tendency, reflecting mainly the degree of open fractures (red = the highest expansion tendency, blue = second, and yellow = the lowest). This coincides with the principal stress direction, suggesting the EW strike of effective open fractures, as confirmed by drilling results.

Fracture network modeling

Fracture network modeling constructs a 3D model of a geological body through fracture modeling and calculating fracture porosity and permeability. This directly aids exploration, production, and development, as well as the design of horizontal wells, well branches, and highly deviated wells. The calculation of reservoir permeability and porosity follows fracture modeling and provides a basis for reserve calculation and drilling optimization.

Visualized characterization of fracture network

As demonstrated in Xinchang, "weak and discontinuous" amplitudes in seismic profiles occur at high-producing gas wells. Areas where P-waves and C-waves are both weak and discontinuous coincide with higher reservoir fracture density and better gas production. To display the distribution of the weak and discontinuous amplitudes in the data volume, a geobody is calculated to visualize reservoir connectivity and shapes. This allows further targeting of weak amplitudes in Xinchang.

Figure 12 shows a seismic line between wells with targeted areas highlighted. Geobody analysis performed on the TX_2^4 reservoir section of Xujiahe Member 2 highlighted the connectivity of weak and discontinuous amplitudes, which may represent the connectivity of reservoirs due to fractures.

Section	Sand	Curvature Attribute		S-wave Splitting		P-wave Azimuthal Anisotropy	Coherency
		Class 1	Class 2	Class 1	Class 2		
Xujiahe Member 4	TX_4^8	>5	>7				<60
	TX_4^9						
Xujiahe Member 2	TX_2^2	>3	>2.6	Blue zone	Blue + green zone	>1.06	<50
	TX_2^3	>3	>2.6				
	TX_2^4	>3	>2.6	Blue zone	Blue + green zone		
	TX_2^5	>3.6	>3			>1.09	
	TX_2^6	>4.6	>4				
	TX_2^7	>6	>5				

Table 1. *Parameters for overall appraisal of fractures in Xinchang.*

Figure 13, a 3D visualization of the incoherent anomalies, clearly shows the distribution of the discontinuous reflections in 3D space. This type of representation was important for designing horizontal well 10-1H. Horizontal well drilling was designed to maximize intersection with discontinuous reflections zones in order to penetrate thicker fractured reservoir sections.

Integrated prediction and appraisal of fracture development zone

Fracture detection is difficult, and any approach has strengths and weaknesses. Depending solely on a single method to determine the distribution of fractures may result in multiple ambiguous solutions. It is therefore important to gather results from different technologies for a comprehensive answer.

Integrated fracture detection was performed on seven reservoir layers in Xujiahe Member 2 and two fractured reservoir layers at the bottom of Xujiahe Member 4. The work integrated results from seismic curvature, dip angle, similarity, P-wave azimuthal anisotropy prediction, and S-wave splitting fracture prediction, and was calibrated with the fracture analysis from the well data. Fracture indicators were divided into two classes: class 1 fractures are the strongest indicators and class 2 fractures are intermediate indicators, as follows:

- Zones with lower-fracture density exhibit class 2 indicators;
- Zone with high-facture density exhibit class 1 indictors.

Fracture prediction parameters for different reservoirs should be different because of the difference in structure and lithology at different layers, as well as varying degrees of fault development. For example, the folds of Member 4 are broader than those of Member 2, as shown with the different attribute thresholds in Table 1.

Fracture detection by integrating all available information was used for statistical analysis on the cumulative thickness of effective fractures to determine the predicted fracture density for the area and revealed optimum well locations for further drilling.

Results

The use of full-wave data integrated with geological and production information enabled describing the lateral extent of the reservoirs, predicting the effective fracture distribution, and identifying and quantifying natural gas reserves in the Xinchang gas field. Beginning in 2006, the results from these efforts were used to select new exploratory well locations (Figure 14). By the end of 2008, 18 wells had been designed, and five out of the six completed wells had production rates of up to 18.4 MMCF per day. Overall, drilling success in Xinchang has increased from 50% to greater than 80%. Encouraged by the effectiveness at Xinchang, a new 3D/3-C project was designed for the Hexingchang-Gaomiaozi area east of Xinchang. The 500 km^2 seismic survey was completed using digital multicomponent sensors in early 2009. Those data are currently being processed.

New acquisition parameters improved azimuthal coverage and increased fold to 128. Additional exploration benefits from this new full-wave project are expected.

Conclusions

The reservoirs of the Upper Triassic Xujiahe Formation of the western Sichuan Basin have some of the lowest porosities and permeabilities in the world. Due to the depth of the reservoirs, low porosity and permeability, very high velocities, and overpressure, conventional seismic exploration failed to image the fracture zones necessary for production.

Full-wave seismic attributes significantly improved the ability to image the deep-fractured. tight-gas reservoirs of Xinchang. The 3D/3-C full-wave data also provided better understanding of the deep fractured reservoirs of western Sichuan. The achievements described in this paper show that this approach holds promise. One advantage of multicomponent data is the amount of information available to the interpreter and the flexibility to find the right solution. However, the amount of information is also a disadvantage, so it is necessary to streamline interpretation. Further development of 3D/3--C interpretation technologies and increased data-processing capacity are necessary before full-wave and multicomponent technology can become widely used.

Suggested reading. "Azimuthal Anisotropy of 3D Compressional wave seismic data, Weyburn field, Saskatchewan, Canada" by Jenner (PhD dissertation, Colorado School of Mines, 2001). "Exploratory theory and practice of tight gas-bearing clastic rock zones in western Sichuan Basin, Yang Keming, and Xujin" by Zhengwu (in *Gas Reservoir Formation Theory and Exploration Development Technology*, Geological Publishing House, Beijing, 2004). TLE

Corresponding author: tjm@tjm01.com